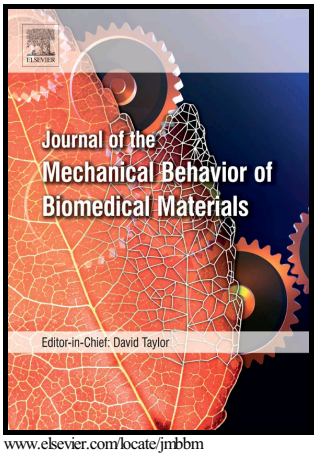

www.elsevier.com/locate/jmbbm

Biomechanical properties and microstructure of neonatal porcine ventricles

Faizan Ahmad, R. Prabhu, Jun Liao, Shwe Soe, Michael D. Jones, Jonathan Miller, Parker Berthelson, Daniel Enge, Katherine M. Copeland, Samar Shaabeth, Richard Johnston, Ian Maconochie, Peter S. Theobald

PII: S1751-6161(18)30592-7
DOI: https://doi.org/10.1016/j.jmbbm.2018.07.038
Reference: JMBBM2906

To appear in: *Journal of the Mechanical Behavior of Biomedical Materials*

Received date: 17 November 2017
Revised date: 26 June 2018
Accepted date: 27 July 2018

Cite this article as: Faizan Ahmad, R. Prabhu, Jun Liao, Shwe Soe, Michael D. Jones, Jonathan Miller, Parker Berthelson, Daniel Enge, Katherine M. Copeland, Samar Shaabeth, Richard Johnston, Ian Maconochie and Peter S. Theobald, Biomechanical properties and microstructure of neonatal porcine ventricles, *Journal of the Mechanical Behavior of Biomedical Materials,* https://doi.org/10.1016/j.jmbbm.2018.07.038

Biomechanical properties and microstructure of neonatal porcine ventricles

Faizan Ahmad[1], R. Prabhu[2], Jun Liao[2, 3*], Shwe Soe[1], Michael D Jones[1], Jonathan Miller[2], Parker Berthelson[2], Daniel Enge[4], Katherine M. Copeland[3], Samar Shaabeth[1], Richard Johnston[5], Ian Maconochie[6], Peter S. Theobald[1*]

[1] School of Engineering, Cardiff University, UK;
[2] Centre for Advanced Vehicular Systems and Department of Biological Engineering, Mississippi State University, US;
[3] Department of Bioengineering, The University of Texas at Arlington, US;
[4] University of the Cumberlands, US;
[5] College of Engineering, Swansea University, UK;
[6] Imperial College NHS Healthcare Trust, UK.

Corresponding author:

Jun Liao, PhD, FAHA
Associate Professor,
Department of Bioengineering,
University of Texas at Arlington,
500 UTA BLVD, Suite 353,
Arlington, TX 76010,
Phone: (817) 272-6779
Email: jun.liao@uta.edu

Peter S Theobald, PhD
Bioengineering Research Group
Cardiff School of Engineering, Cardiff University,
Queens Buildings,
The Parade, Newport Road,
Cardiff, CF243AA, UK,
Phone (44) 2920 874726
Email: TheobaldPS@cardiff.ac.uk

Highlights

- Maturation increases the stiffness of cardiac tissue when comparing our neonatal data to that describing the mature porcine heart.
- Neonatal tissue exhibits non-linear, anisotropic, and heterogeneous behaviour.
- The neonatal porcine cardiac tissue is one-half the uniaxial stiffness, one-third the biaxial stiffness, and one-fourth the simple shear stiffness, of equivalent mature tissue.
- The anterior walls are stiffer than the posterior walls, in both ventricles.

Abstract

Neonatal heart disorders represent a major clinical challenge, with congenital heart disease alone affecting 36,000 new-borns annually within the European Union. Surgical intervention to restore normal function includes the implantation of synthetic and biological materials; however, a lack of experimental data describing the mechanical behaviour of neonatal cardiac tissue is likely to contribute to the relatively poor short- and long-term outcome of these implants. This study focused on characterising the mechanical behaviour of neonatal cardiac tissue using a porcine model, to enhance the understanding of how this differs to the equivalent mature tissue. The biomechanical properties of neonatal porcine cardiac tissue were characterised by uniaxial tensile, biaxial tensile, and simple shear loading modes, using samples collected from the anterior and posterior walls of the right and left ventricles. Histological images were prepared using Masson's trichrome staining, to enable assessment of the microstructure and correlation with tissue behaviour. The mechanical tests demonstrated that the neonatal cardiac tissue is non–linear, anisotropic, viscoelastic and heterogeneous. Our data provide a baseline describing the biomechanical behaviour of immature porcine cardiac tissue. Comparison with published data also indicated that the neonatal porcine cardiac tissue exhibits one-half the stiffness of mature porcine tissue in uniaxial extension testing, one-third in biaxial extension testing, and one-fourth stiffness in simple shear testing; hence, it provides an indication as to the relative change in characteristics associated with tissue maturation. These data may prove valuable to researchers investigating neonatal cardiac mechanics.

Keywords: Neonatal porcine hearts, cardiac mechanics, congenital heart diseases, passive mechanical behaviour, age-dependent variations.

1. Introduction

Congenital heart disease (CHD) annually affects approximately 36,000 new-borns within the European Union [1, 2], and describes a series of structural cardiac disorders, including ventricular and atrial septal defects. Multi-physics modelling and the development of new synthetic materials are innovative approaches seeking to positively influence the clinical outcomes; however, an acute lack of data describing the biomechanical behaviour of neonatal cardiac tissue, twinned with the structural changes to the tissue during maturating, is potentially limiting the effectiveness of these novel techniques.

The adult cardiac tissue is known to exhibit highly complex behaviour, including non-linearity and anisotropy [3-10], as a consequence of its intricate structure [11-15]. Critically, ventricular wall functionality differs between the adult and neonate, as the latter can only increase the cardiac output by increasing the heart rate (although only limited), whereas the adult heart can also increase stroke volume [16, 17]. The neonate heart also has a greater fraction of fibrous tissue to contractile tissue, than an adult [16, 17], whilst there is variation in the collagen fibril density, and mono-nucleated and bi-nucleated cell concentrations [18-20]. Increasing age is also associated with changes in the cardiac matrix, and an increase in collagen fibril crosslinking and assembly [21]. No experimental data exists to quantify neonate tissue, however, meaning simulations adopt and/or scale adult data, incorporating an unknown level of error [21-24].

Computational modelling is increasingly used in adult cardiology to understand the behaviour of structural components, enabling the simulation of normal and pathophysiological conditions and leading to new interventions [25-31]. A lack of appropriate data to describe neonatal tissue limits the widespread use and effectiveness of sophisticated techniques, to investigate neonatal-based disorders. Surgical intervention, aiming to restore normal function, includes the implantation of synthetic materials to mimic natural tissue behaviour [32-34]; however, the relatively poor short- and long-term

outcomes may be partly associated with the scant literature describing neonatal cardiac biomechanics. This lack of knowledge may also be contributing to the relatively limited success of biological scaffolds [35, 36]; hence, enhanced knowledge of tissue behaviour to achieve more effective designs has the potential to positively influence CHD mortality and morbidity [36].

We thus aim to systematically quantify the biomechanical properties of neonatal right and left ventricles, using an accepted neonatal porcine animal model [37-44]. These biomechanical data are consolidated with histological imaging, to provide a comprehensive analysis of tissue from the right and left ventricle free walls (RVFW, LVFW). This study will provide baseline data describing the behaviour of neonatal porcine tissue and, through comparison to equivalent mature data, will also be able to provide an insight into the effect of maturation on tissue behaviour. Such data may then prove useful to those researchers investigating immature cardiac tissue mechanics and the clinicians/bioengineers exploring new intervention techniques in congenital heart diseases.

2. Materials and methods

2.1. Materials

Forty-three, one-day-old neonatal porcine hearts (Yorkshire) were acquired from a local abattoir house in Mississippi, from donor piglets mass: 2.0 – 2.2kg, length: 0.35 – 0.48m. The deceased piglets all appeared fully developed, meaning that they were most likely to have died from hypoxia either during or immediately after, farrowing (i.e. birth). All donor's hearts were presumed to be healthy, pending subsequent inspection. The piglets were collected within hours of their death and transported to the Tissue Bioengineering Laboratory at the Mississippi State University, stored in ice-cooled boxes at 4^{o}C. The hearts were then promptly dissected out and visually examined for any macroscopic damage or disruption, with any that failed this assessment being excluded from further investigation. The anterior and posterior aspects of the LVFW and RVFW were then identified (Fig. 1), before defining the FSN-coordinate system as the fibre axis (F), defined as the mean-fibre direction as observed by the external surface texture; the sheet axis (S), defined as the direction transverse to the fibre axis within the layer; the sheet-normal axis (N), defined as the direction perpendicular to both the fibres and layers [9, 10, 45]. In this study, the fibre axis (F) is described as the 'mean-fibre direction' (MFD), and sheet-normal axis (N) as the 'cross fibre direction' (CFD) [10]. Such a method is inherently subjective, though was performed in a manner consistent with previous studies [9, 10].

Uniaxial extension testing samples were dissected from twenty hearts. Ten randomly selected hearts had samples of dimensions 20mm (l) x 10mm (w) x 3mm (t) dissected, with the longest dimension aligned to the MFD. The remaining 10 hearts were used to harvest samples in the CFD (Fig. 2 (a), (b) & (c)). All 20 samples were then trimmed using a cutting punch, achieving a traditional dog-bone shape and a 5mm minimum width. For biaxial extension analysis, five samples (15 x 15 x 3mm) were dissected using a square-shaped

cutting punch from the LVFW, and a further five hearts used for RVFW samples (Fig. 2 (d) & (e)). Each sample was dissected such that the presumed MFD and CFD were consistent with the x- and y-axes of the cutter. A similar approach, though smaller cutter (3 x 3 mm), was adopted to dissect tissue for shear analysis. These were collected from the anterior and posterior aspects of the LVFW and RVFW, dissected from the equatorial regions of 5 hearts (Fig. 2 (f) & (g)). The final eight hearts were used for histological analysis (Fig.1). Thirty-two cubic samples (5 × 5 x 5 mm) were dissected using a square-shaped cutter from the equatorial regions of the anterior and posterior aspects of LVFW and RVFW (Fig. 1). In this instance, a coordinate system was established that ensured consistent orientation of the cutter, as this analysis served to quantify the relative fibre alignment. Hence, the cutter was always aligned with the vertical axis of the heart, defined as passing through the apex and base.

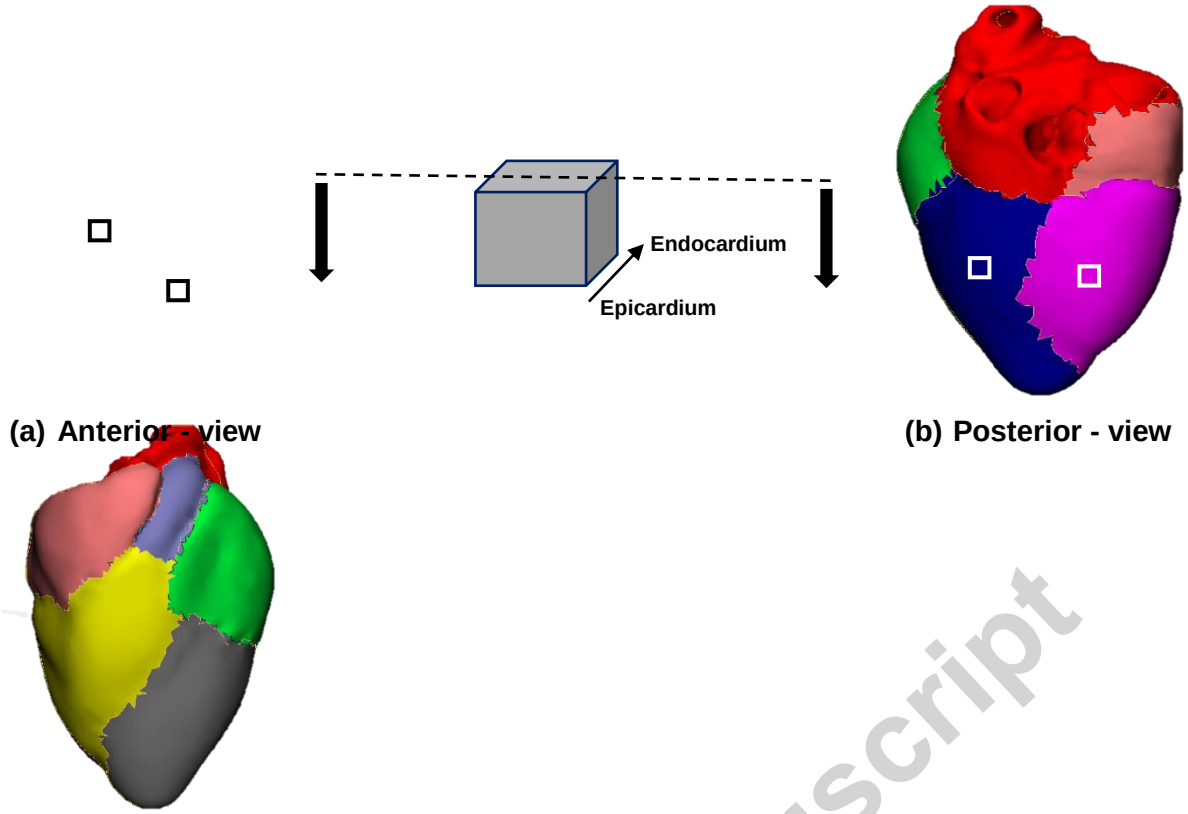

Fig.1. Three-dimensional schematic model of the neonatal porcine heart. **(a)** Anterior view: LVFW = Grey region, RVFW = Yellow region. **(b)** Posterior view: LVFW = blue region, RVFW = pink region. Squares represent the location of dissecting histological samples (5 × 5 x 5mm), which were then sectioned in the plane perpendicular to the transmural direction.

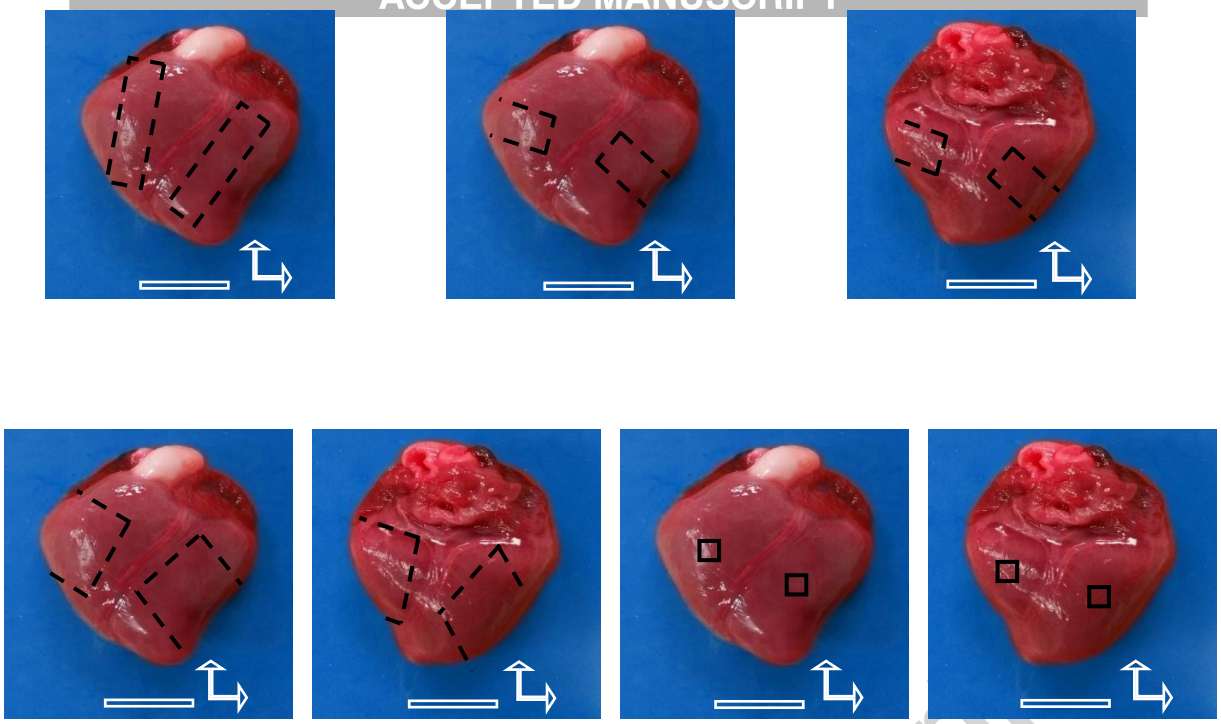

Fig. 2. Schematic representation of the samples harvested from the neonatal porcine heart. Samples were dissected aligned to the 'mean fibre direction' (MFD) and 'cross fibre direction' (CFD), determined by observing the external features of the organ. **(a)** Uniaxial CFD samples are dissected from the anterior aspect of the LVFW and RVFW. **(b) & (c)** Uniaxial MFD samples extend from the anterior to posterior aspect of the LVFW and RVFW. **(d) & (e)** Biaxial (square) samples extended from the anterior to posterior aspects of the LVFW and RVFW. **(f) & (g)** Simple shear samples were dissected from the equatorial region of both the anterior and posterior aspects of the LVFW and RVFW. Scale bar = 12 mm.

2.2. Methods

The directional anisotropy of the LVFW and RVFW tissue was investigated at different deformation states, via four independent protocols. Biomechanical testing was completed within 12h of birth, to produce data from fresh tissue.

2.2.1. Microstructural analysis

All 32 samples were fixed in 4% paraformaldehyde for 48h and then in 70% glutaraldehyde. Samples were then processed through a standard histological preparation protocol, including being dehydrated in graded alcohol, cleared with xylene and then embedded within paraffin wax. Each block was cut perpendicular to the transmural direction, with a 2mm deep section selected for analysis (Fig. 1). A standard Masson's trichrome staining protocol was performed, with the sections finally mounted with Permount. The Masson's trichrome stain identified muscle fibres in red, and collagen fibres light blue.

2.2.2. Uniaxial extension test

Both ends of the dog-bone-shaped samples were wrapped in emery paper and clamped into the stainless steel grips of a uniaxial testing machine (Mach-1; Biosyntech, MN). This produced samples with a dimension of approximately 15mm (l) x 5mm (w) x 3mm (t), with five measurements taken with digital callipers. Each sample was preconditioned with 10 cycles at 10% strain, before being loaded to failure at 1.5 mms^{-1} ramp speed. Engineering stress was computed by normalising the applied force to the initial cross-sectional area, and engineering strain calculated by normalising the displacement to the initial gauge length. Mean peak stress, which describes the stress of failure, was then calculated from these data for the MFD and CFD samples. The last preconditioning cycle

was used to quantify the myocardial hysteresis (to account for energy dissipation due to the viscoelastic behaviour), dividing the area enclosed by the loading and unloading curves (energy dissipation) by the area beneath the loading curve (energy input).

2.2.3. Biaxial extension test

Biaxial mechanical properties were investigated using a biaxial testing system, described in detail elsewhere [46, 47]. The square samples, which had been dissected with the observed MFD and CFD aligned with the x- and y-axes were then mounted onto the machine using surgical sutures. Five thickness measurements were collected at different locations, using a digital calliper, to determine an average dimension. The samples were then immersed in 37^{o}C PBS. Ten preconditioning cycles were performed before the data were collected for analyses. The specimens were stretched by applying a 30 N/m tension in the MFD (T_{MFD}) and CFD (T_{CFD}) at 0.5 mms^{-1}. Tissue deformation was measured via a charge-coupled device camera (National Instrument, IMAQ CCD, Austin, TX), tracking the relative position of four reference points placed in a 2 × 2 array. In-house Labview code (National Instrument, Version 6, Austin, TX) was used to control the stepper motors and record the applied forces and tissue strain.

2.2.4. Simple shear test

Simple shear tests focussed on the relative shearing and sliding of the myocardial tissues. Simple shear tests involved mounting the tissue in custom-built shear plates which, in turn, were mounted in the Mach 1 testing machine (Biosyntech, MN) and submerged in PBS at 37°C. Regional anisotropy was investigated using 3 × 3 x 3 mm cubic specimens that had been dissected such that the MFD and CFD were consistent with the x and y-axes. Tissue samples were mounted between the two shear plates using minimal cyanoacrylate. They were sheared in the FS plane along the MFD and then the NS plane along the CFD,

following identification of these planes representing the extremes of shear behaviour in the adult porcine LVFW myocardium [9]. The tissue was exposed to positive and negative shear at 10% and incrementally increased to a maximum 50%, at a loading rate of 0.02 mms^{-1}.

2.3. Data analysis

2.3.1. Fibre orientation and surface area calculations from histological images

The Fourier components analysis method quantified the fibre orientation from histological images of the 4 heart regions, using the Fiji/Image J (NIH, USA) software and the 'Directionality' plug-in (https://imagej.net/Directionality) [48]. Data from histological images enabled identification of the 'preferred' fibre orientation direction (i.e. the histogram peak). This peak was then fitted with a Gaussian function, reporting the preferred fibre orientation [49, 50]. A custom MATLAB code was also adopted to quantify the surface area ratio of collagen to myocyte fibres, using image thresholding based on RGB (red, green and blue) values [51].

2.3.2. Uniaxial and biaxial tensile tests

Engineering stresses in MFD (P_{11}) and CFD (P_{22}) are calculated as the ratio of the applied force and the initial cross-sectional area. Strains in the MFD (ε_1) and CFD (ε_2) are computed as the ratio of the displacement and the initial gauge length.

$$\mathrm{P}_{11} = \frac{\mathrm{f}_1}{\mathrm{A}_1}, \qquad \mathrm{P}_{22} = \frac{\mathrm{f}_2}{\mathrm{A}_2}, \tag{1}$$

$$\varepsilon_1 = \frac{\mathrm{x}_1}{\mathrm{X}_1}, \qquad \varepsilon_2 = \frac{\mathrm{x}_2}{\mathrm{X}_2},$$

Where: (x_1, x_2) are the displacements; (X_1 , X_2) are the initial gauge lengths.

2.3.3. Simple shear test

Shear stress (τ) is the ratio of the shear force f and the shear area $a = L^2$; hence, this calculation represents the relative in-plane displacement of two parallel layers of this cubic specimen. The amount of shear γ ranges from 0.1 – 0.5 in increments of 0.1, whilst the separation distance (side length) for the cubic specimen was L ~ 3 mm.

$$\gamma = \frac{\Delta L}{\mathrm{L}}, \qquad \tau = \frac{f}{L^2}, \tag{2}$$

Where: ΔL represents the shear displacement.

2.3.4. Statistical analysis

All values are reported as the mean ± standard deviation (SD), where a *p*-value less than 0.05 was considered as statistically significant. One-way analysis of variances (ANOVA) was performed along with Tukey HSD post hoc test to quantify the statistical significance of the anterior and posterior aspects of both ventricles. All statistical analyses were conducted in SPSS 20.0.

3. Results

3.1. Microstructural analysis

Representative images from the microscopic examination are presented showing the overall fibre orientation in the anterior and posterior aspects of the LVFW and RVFW (Fig. 3). These samples were collected aligned to the vertical axis of the heart (defined as passing through the apex and base). The images indicate that the fibre direction in the anterior LVFW are more aligned to the horizontal, and posterior the vertical axes, respectively. Indeed, the alignment of fibres with either the horizontal or vertical appears stronger in the LVFW than the RVFW. The Fourier component analysis quantifies these alignments and confirms that the fibres in the anterior and posterior LVFW are more aligned to the horizontal and vertical axes of the heart. Conversely, fibres in the anterior and posterior RVFW are aligned nearer diagonally (Table 1), though the former has less intercellular space (Figs. 3 (c) & (d)). The ratio of collagen to myocyte fibres was highest in the LVFW posterior, and lowest in the RVFW anterior, regions (Table 2). The average in-plane (x, y) principal (preferred) fibre orientation of the LVFW and RVFW are stated in Table 1.

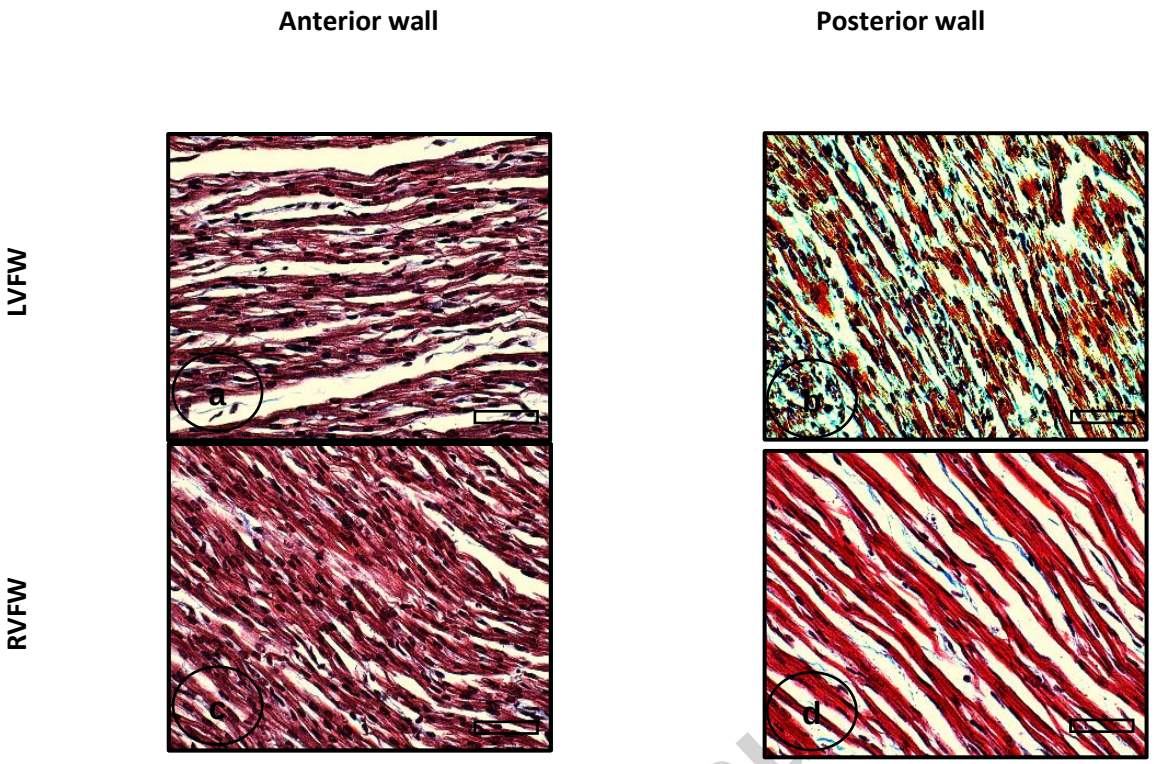

Fig. 3. Masson's trichrome staining images of the neonatal porcine heart sectioned from the plane perpendicular to the transmural direction and viewed at × 40 magnification. **(a)** LVFW anterior, demonstrating circumferentially aligned fibres. **(b)** LVFW posterior, describing longitudinally aligned fibres. The RVFW anterior **(c)** and posterior **(d)** aspects demonstrated almost symmetrical fibre alignment, with the former having greater concentration and alignment of muscle fibres as reported in Table.2. Principal or preferred fibre angles are detailed in Table.1. Scale bar = 50µm.

Heart regions	Preferred fibre orientation μ (º)	(SD)	Coefficient of determination R^2	(SD)
LVFW (A)	4.19	(0.6)	0.96	(0.4)
LVFW (P)	-60.98	(0.7)	0.98	(0.6)
RVFW (A)	-40.77	(0.2)	0.98	(0.7)
RVFW (P)	-44.01	(0.4)	0.98	(0.6)

Table 1

The average in-plane (x, y) principal fibre orientation parameter and coefficient of determination R^2 'goodness of fit' for RVFW and LVFW in the anterior (n = 16) and posterior (n = 16) aspects. Histological specimens were examined in the plane perpendicular to the transmural direction, using Fourier components analysis method (n = 32).

Collagen / myocyte	LV (A)	(SD)	LV (P)	(SD)	RV (A)	(SD)	RV (P)	(SD)
Transmural - plane	0.10	(0.5)	0.20	(0.6)	0.03	(0.3)	0.08	(0.4)

Table 2

The average surface area ratio of collagen to myocyte for RVFW and LVFW in the anterior (n = 16) and posterior (n = 16) aspects. Histological specimens were examined in the plane perpendicular to the transmural direction, using custom MATLAB code.

3.2. Uniaxial extension behaviour

The mean uniaxial behaviour of the LVFW and RVFW in extension is presented in Fig. 4 (a), with the data describing a non–linear, anisotropic, viscoelastic (hysteresis – formation) response in all regions. Ten preconditioning cycles were performed, with both the LVFW and RVFW demonstrating the greatest change in behaviour during the first two cycles (Fig. 4 (b) & (c)). It is evident from Figs. 4 (a), (d), (e) & (f) that the MFD was stiffer than the CFD in the strain range 0 to ~ 0.20, but that the CFD becomes stiffer than the MFD after ~ 0.20 for both ventricles. The RVFW is consistently the stiffer of the two ventricles. The energy dissipation and failure stresses are reported in Tables. 3 & 4. The data in Figs. 4 (a) – (f) demonstrate similar trends, though there is a significant difference between the RVFW and LVFW peak stresses ($p = 0.001$) and between MFD and CFD ($p = 0.0001$).

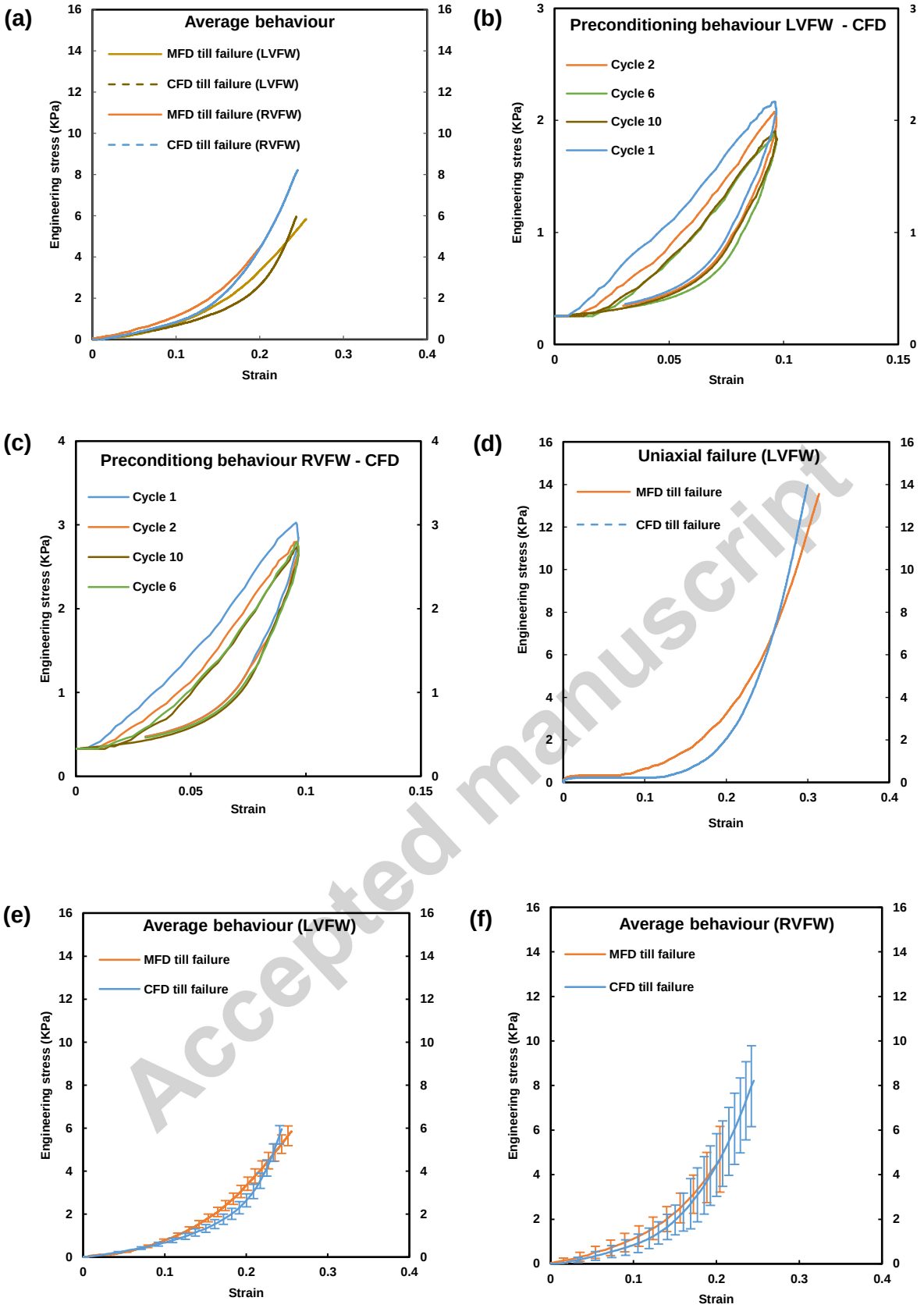

Fig. 4. (a) Average 'uniaxial behaviour' of LVFW & RVFW until failure (n = 5). **(b) – (c)** Uniaxial cyclic behaviour of LVFW and RVFW in CFD. **(d)** Representing passive 'uniaxial

behaviour' of LVFW until failure. Mean curves of the LVFW **(e)** and RVFW **(f)** (n = 5).

Standard deviation indicated by error bars.

	Hysteresis area			
Heart regions		(SD)	CFD	(SD)

	MFD			
LVFW	91	(112)	80	(82)
RVFW	54	(108)	43	(93)

Table 3

Average hysteresis area (J/m^3) of neonatal porcine LVFW and RVFW for uniaxial testing at 20% strain in MFD and CFD.

Heart regions	MFD	(SD)	CFD	(SD)
LVFW	5.84	(0.4)	5.95	(0.4)
RVFW	4.69	(1.4)	8.22	(1.8)

Table 4

Average failure stress values (KPa) for neonatal LVFW and RVFW for uniaxial testing; the specimens were stretched until failure. Mean ± SD stress values are plotted in Figs. 4 (e) and 4 (f).

3.3. Biaxial extension behaviour

The biaxial mechanical representatives (Engineering stress vs stretch) were investigated at 30 Nm^{-1}: 30 Nm^{-1} tension ranges (Fig. 5). RVFW and LVFW possess non–linear, anisotropic and viscoelastic (hysteresis formation) mechanical responses (Figs. 5 (a) – (b)). The RVFW is stiffer, whilst the LVFW demonstrates greater viscoelasticity. The MFD exhibits stiffer behaviour and greater viscoelasticity in both ventricles, than the CFD (Figs. 5 (a) – (d)). The LVFW exhibits mechanical cross-coupling between the MFD and CFD as demonstrated in Fig. 5(a). The energy dissipation and peak Engineering stresses are presented in Tables. 5 & 6. A significant difference exists between the RVFW and LVFW peak Engineering stresses in MFD ($p = 0.0001$) and CFD ($p = 0.0001$).

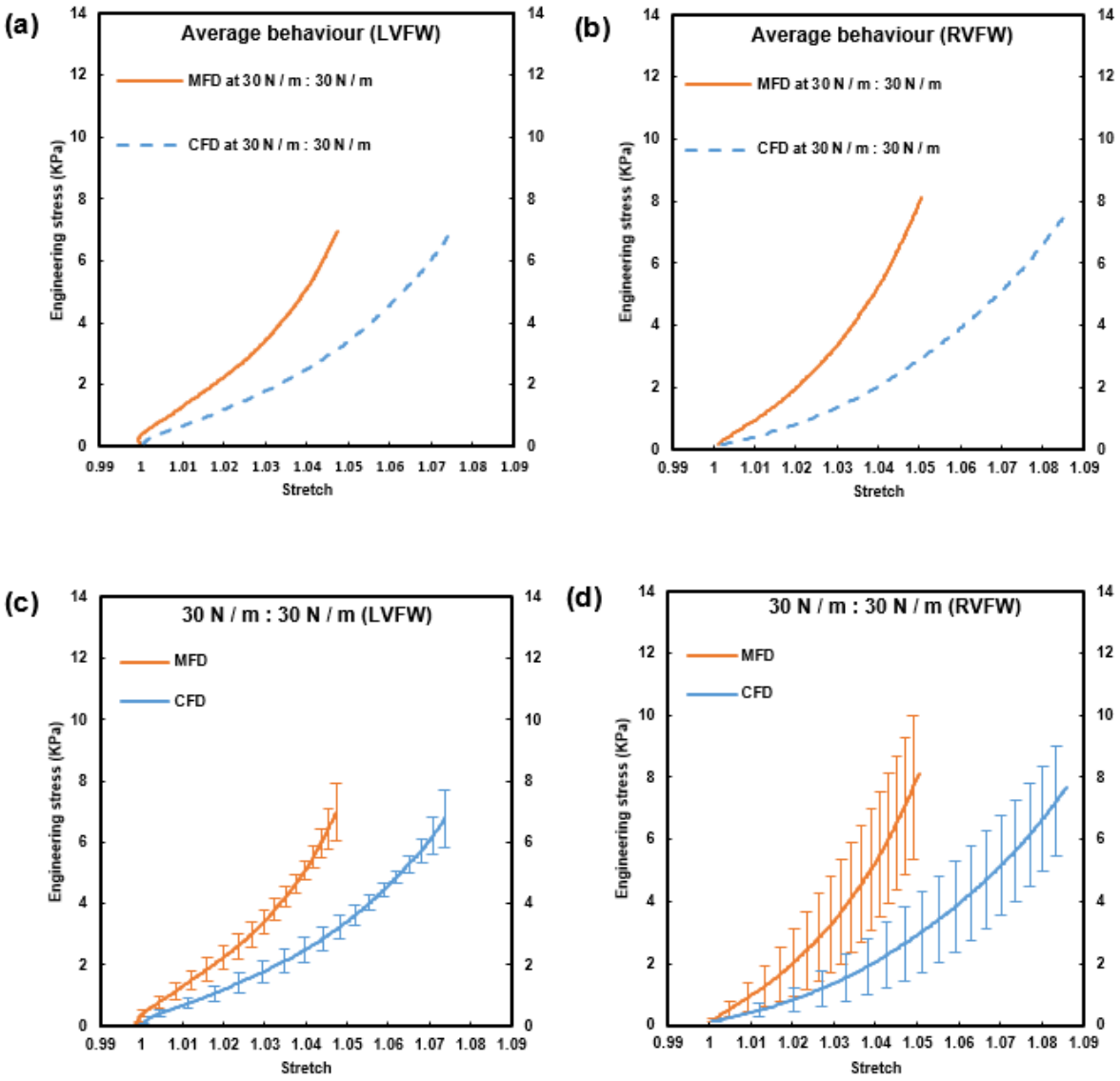

Fig. 5. (a) The average biaxial behaviour of LVFW, with negative strain indicating possible in-plane mechanical cross-coupling between the MFD-CFD (n = 5). **(b)** Average biaxial behaviour of RVFW (n = 5). Mean 'biaxial' curves of the **(c)** LVFW and **(d)** RVFW (n = 5). Error bars describe the standard deviation.

Hysteresis area				
Heart regions	MFD	(SD)	CFD	(SD)
LVFW	51	(121)	19	(76)
RVFW	48	(128)	23	(67)

Table 5

Average hysteresis area (J/m^3) of neonatal porcine LVFW and RVFW for biaxial testing at (30:30) N / m in MFD and CFD.

Heart regions	MFD	(SD)	CFD	(SD)
LVFW	6.97	(0.9)	6.77	(0.9)
RVFW	8.11	(2.3)	7.67	(1.8)

Table 6

Average peak Engineering stress values (KPa) for neonatal porcine LVFW and RVFW for biaxial testing at (30:30) N / m in MFD and CFD. Mean ± SD stress values are plotted in figs. 5 (c) and 5 (d).

3.4. Simple shear behaviour

Hysteresis formation (energy dissipation) is prominently evident throughout the cyclic shearing behaviour, with both ventricles demonstrating increased shear (Fig. 6). The anterior walls appear stiffer with greater energy dissipation than the posterior walls of both ventricles, whilst the MFD is stiffer than the CFD (Fig. 7 (a) – (b)). The RVFW exhibits asymmetrical behaviour, possessing greater stiffness in the positive direction anteriorly and negative direction posteriorly. Conversely, both aspects of the LVFW exhibit consistent behaviour in both directions (Fig. 6). The energy dissipation and peak shear stresses are described in Tables. 7, 8 & 9. The influence of fibre direction is described in (Figs. 7 (a) – (f)), whilst variations in tissue behaviour are identified statistically via a one-way ANOVA and Tukey HSD post hoc test (Table. 10).

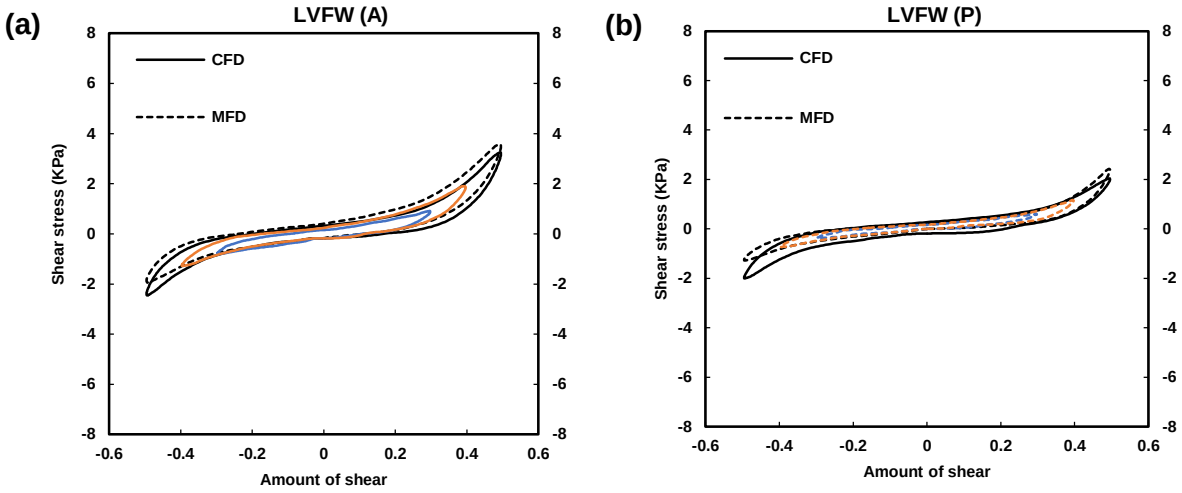

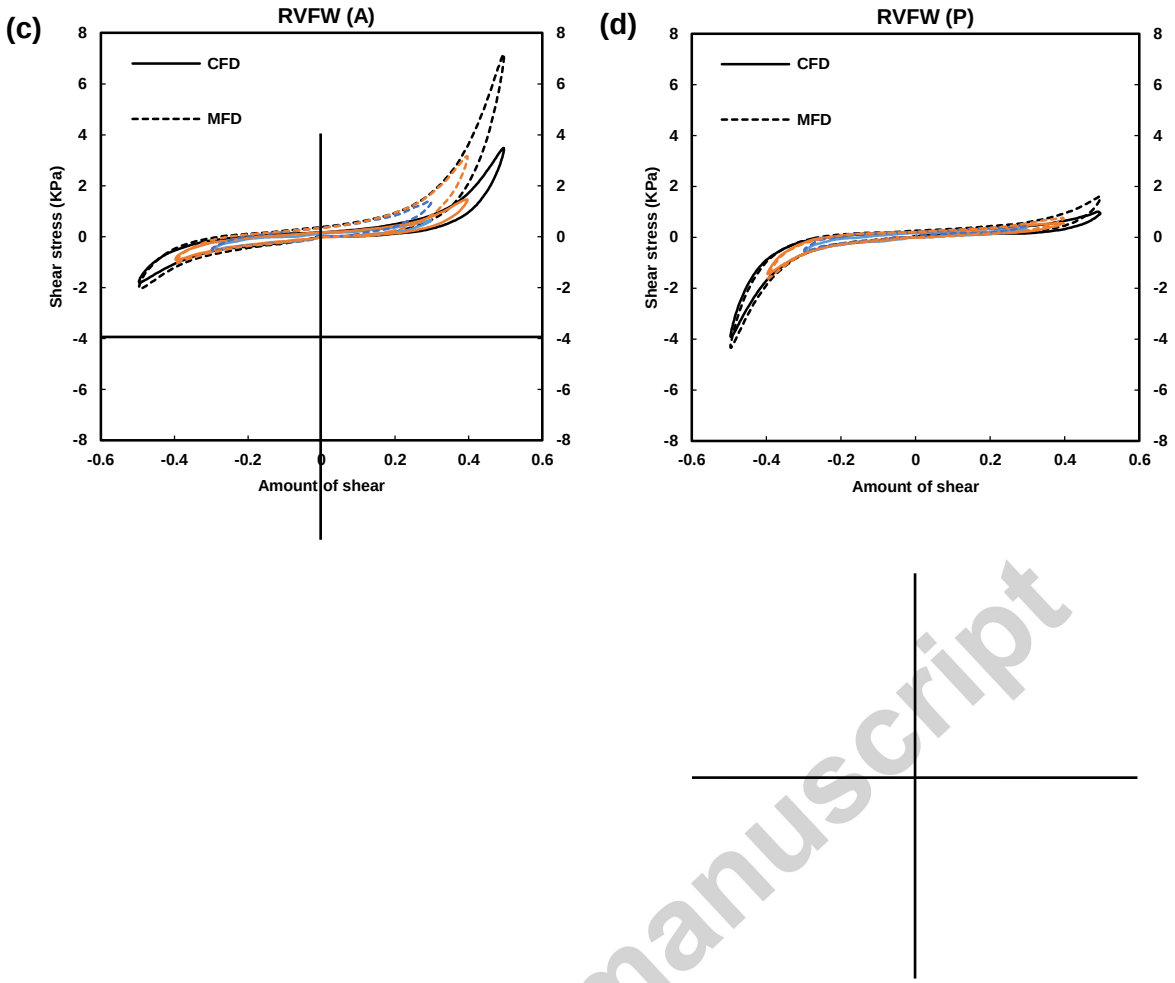

Fig.6. Demonstrating passive 'simple shear' behaviour of the anterior and posterior aspects of the LVFW & RVFW in the MFD and CFD, at increments of 0.3 (blue curve), 0.4 (orange curve) and 0.5 (black curve). The positive y-axis represents the positive direction of myocardial shearing. **(a)** LVFW – anterior. **(b)** LVFW – posterior. **(c)** RVFW – anterior. **(d)** RVFW – posterior.

(a)

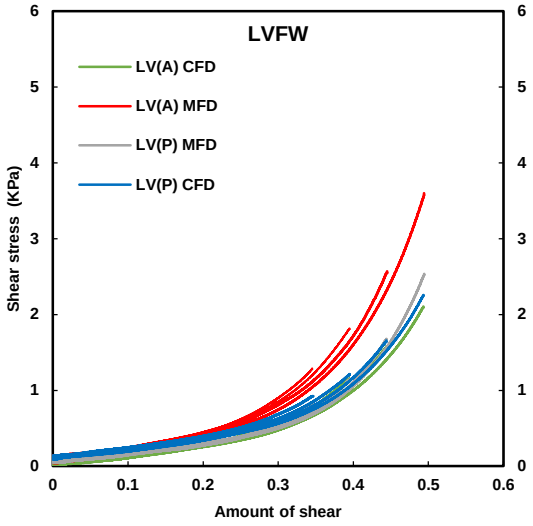

(b)

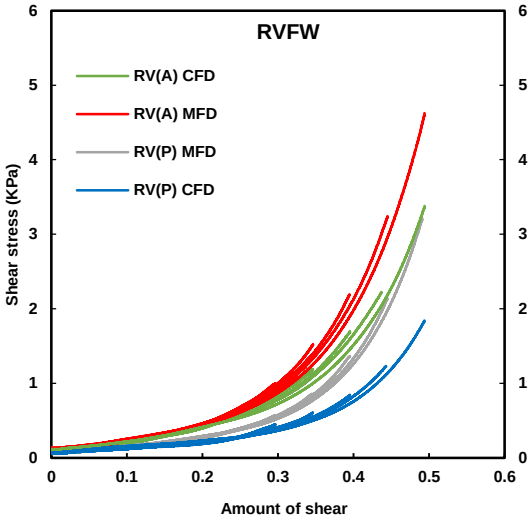

(c)

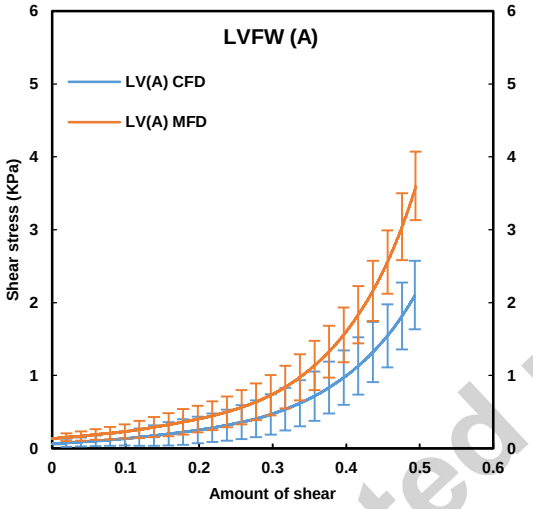

(d)

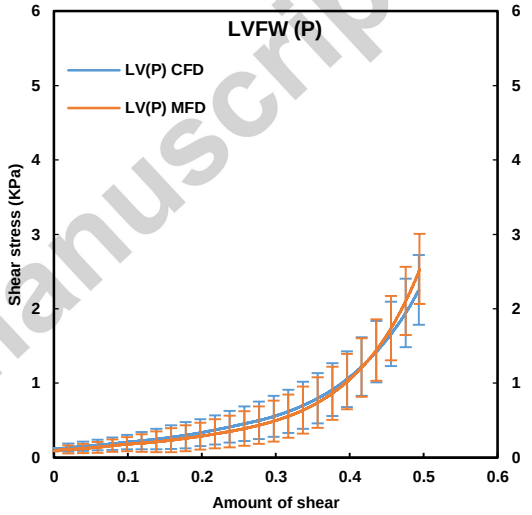

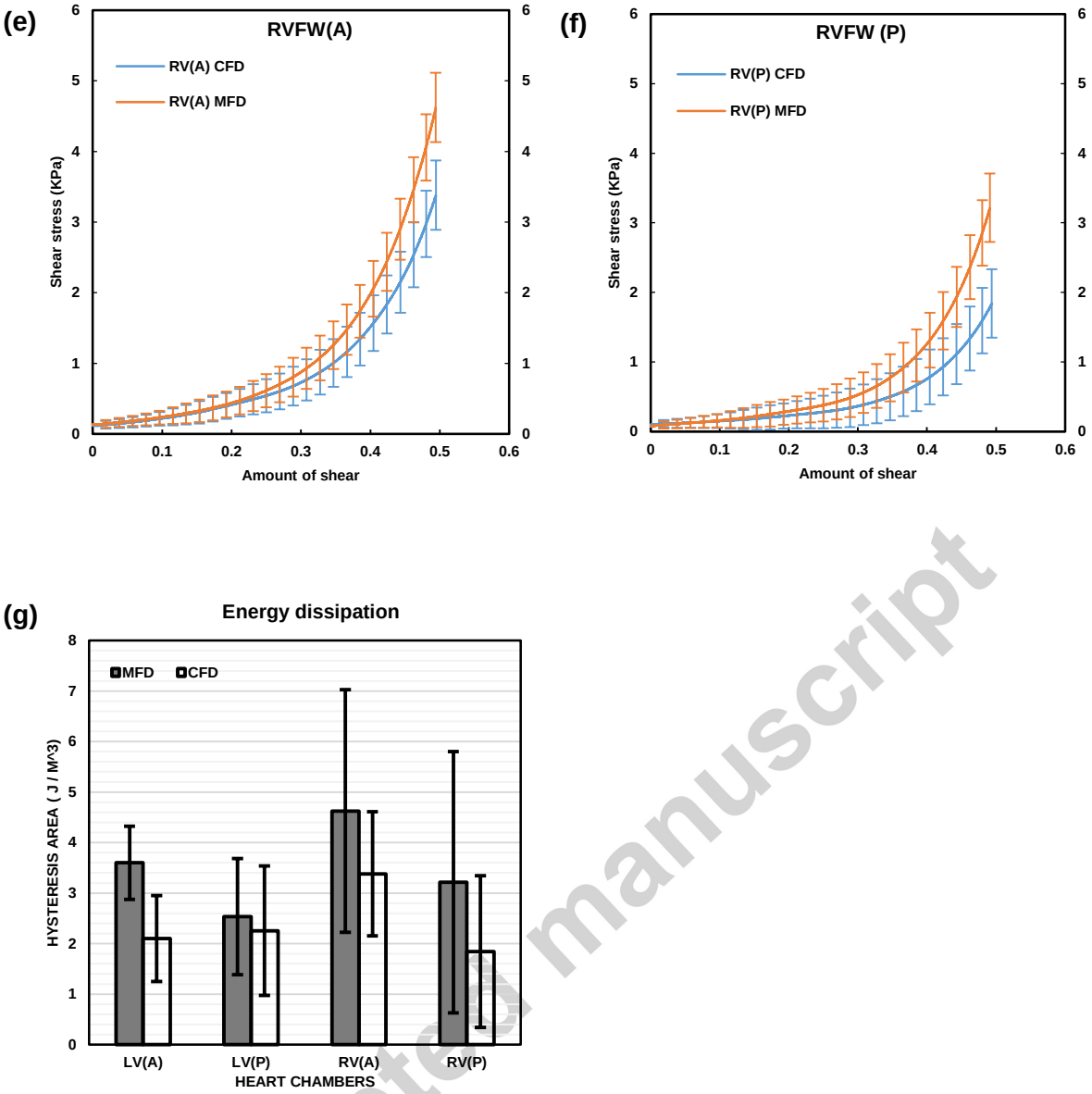

Fig. 7. 'Mean simple shear behaviour' of anterior and posterior aspect of the LVFW **(a)** and the RVFW **(b),** in the MFD and CFD at increments of 0.1, 0.2, 0.3, 0.4 & 0.5 (n = 5). LVFW anterior **(c)** and posterior **(d)** in MFD and CFD, at an increment of 0.5. RVFW anterior **(e)** and posterior **(f)** in MFD and CFD at an increment of 0.5. **(g)** Column plots indicate mean hysteresis areas in the anterior and posterior aspect of LVFW & RVFW, for MFD and CFD at an increment of 0.5 (n = 5). Error bars represent standard deviation.

Hysteresis area				
Heart regions	MFD	(SD)	CFD	(SD)
LVFW (A)	306	(104)	260	(86)
LVFW (P)	201	(17)	187	(59)
RVFW (A)	387	(87)	244	(159)
RVFW (P)	208	(117)	174	(41)

Table 7

Average hysteresis area (J/m^3) of neonatal porcine LVFW and RVFW in anteroposterior directions for simple shear testing at 0.5 increments in MFD and CFD. Mean ± SD energy dissipation values are plotted in Fig. 7 (g).

LVFW (A)	LVFW (P)

Increments	MFD	(SD)	CFD	(SD)	MFD	(SD)	CFD	(SD)
0.3	0.84	(0.2)	0.57	(0.3)	0.55	(0.2)	0.67	(0.2)
0.4	1.82	(0.3)	1.15	(0.4)	1.14	(0.3)	1.22	(0.4)
0.5	3.60	(0.4)	2.10	(0.5)	2.53	(0.4)	2.25	(0.5)

Table 8

Average peak shear stress values (KPa) for the neonatal LVFW in the anterior (A) and posterior (P) aspects for simple shear testing at 0.3, 0.4, 0.5 increments in MFD and CFD modes. Mean ± SD stress values are plotted in Figs. 7 (c) and 7 (d).

	RVFW (A)				RVFW (P)			
Increments	MFD	(SD)	CFD	(SD)	MFD	(SD)	CFD	(SD)
0.3	0.99	(0.2)	0.82	(0.3)	0.56	(0.3)	0.45	(0.4)
0.4	2.19	(0.3)	1.69	(0.3)	1.36	(0.4)	0.85	(0.4)
0.5	4.62	(0.4)	3.38	(0.5)	3.22	(0.4)	1.84	(0.5)

Table 9

Average peak shear stress values (KPa) for the neonatal RVFW in the anterior (A) and posterior (P) aspects for simple shear testing at 0.3, 0.4, 0.5 increments in MFD and CFD modes. Mean ± SD stress values are plotted in Figs. 7 (e) and 7 (f).

	LVFW (A)		LVFW (P)		RVFW (A)		RVFW (P)
Configurations	MFD	CFD	MFD	CFD	MFD	CFD	MFD
1	0.0001	0.0001	0.0001	0.0001	-	-	-
2	-	-	-	-	0.0001	0.0001	0.0001
3	0.0001	0.0001	-	-	0.002	0.01	-
4	-	-	0.86	0.86	-	-	0.12

Table 10

Statistical analysis (One way ANOVA along with Tukey HSD post hoc test) data for RVFW and LVFW in the anterior (A) and posterior (P) aspects represent: (1) LVFW (anterior & posterior) for MFD – CFD; (2) RVFW (anterior & posterior) for MFD – CFD; (3) LVFW (A) and RVFW (A) for MFD – CFD; and (4) LVFW (P) and RVFW (P) for MFD – CFD respectively. P – Value less than 0.05 considered statistically significant.

4. Discussion

This study has identified non–linear, anisotropic, viscoelastic and heterogeneous mechanical behaviour of neonatal porcine ventricle tissue. These overall characteristics are consistent with those of other soft tissues [52-56].

Uniaxial extension testing to failure was performed following ten preconditioning cycles (Figs. 4 (b) & (c)), a method consistent with that reported elsewhere [4, 5, 7, 57-62]. Uniaxial testing for failure of the immature tissue was performed and revealed that the MFD was stiffer and more viscoelastic than the CFD (Figs. 4 (a)). Such a viscoelastic response is common in soft tissues and is due to the fluid-structure interaction within the elaborate microstructure of the cardiac samples [63-65]. At low strains, the myocardial mechanical response appears governed solely by cardiomyocytes. As the tissue was extended beyond 20% however, the CFD became stiffer than the MFD in both ventricles (Fig. 4 (a)). This phenomenon has previously been attributed to the perimysial collagen, which provides some reinforcement of the tissue as it approaches its extensibility limit. This apparent coupling between the cardiomyocytes and collagen fibrils appears to contribute to the mechanical strength of the myocardium [66-68]. A similar function of this collagen was previously

reported in the adventitia of arteries [69-71]. The similar trends of the MFD and CFD uniaxial plots (Fig. 4(a)) demonstrate their similar anisotropic behaviour. Comparison with equivalent mature data indicates this variation is relatively small, probably due to the relatively few collagen fibril crosslinks, which are known to increase with age [3, 19].

Uniaxial testing also demonstrated that the LVFW had greater extensibility and viscoelasticity, though lower stiffness, than the RVFW (Figs. 4(a), (b) & (c)). This is surprising given that the LVFW has a greater proportion of collagen. Our observation, of a greater ratio of collagen to myocyte fibres in the LVFW, is consistent with previous reports of higher collagen content preserving wall thickness during diastole and systole [51, 72-74] (Table 2). Since a higher collagen content would typically be associated with greater stiffness in mature tissues, the less stiff behaviour observed here might be related to the collagen state in a 1-day neonatal heart. This is different to the intuitive mechanical contribution of collagen typical in mature tissues. It is noted that the uniaxial (LVFW – MFD) stiffness of neonatal porcine data reported here (23 kPa) is approximately one-half that of the equivalent mature porcine tissue (47 kPa) [75].

The RVFW demonstrated greater stiffness relative to the LVFW during biaxial testing which may, in part at least, be explained by the greater proportion of muscle fibres to the immature collagen than the LVFW (Fig. 5 & Table. 2). This is also the likely reason for the greater LVFW viscoelasticity, and the RVFW's greater anisotropy, which is consistent with previous data [6]. Both ventricles demonstrated that the MFD was nearly twice as viscoelastic as the CFD (Table 5). Figure 5 (a) (Engineering stress vs stretch) demonstrated slight negative strain in the MFD and CFD. Similar, though stronger, trends have previously been reported in adult mammalian heart tissue [76] and was associated with a dense network of fine collagen fibrils linking the cardiomyocytes and large collagen fibrils. This mechanical coupling may contribute to maintaining the myocardial mechanical stiffness [10, 66]. The mechanical trends between MFD and CFD exhibited in Figs. 5 (a) & (b), is consistent with data from some canine studies [4, 5], though other adult studies report the

MFD as being approximately twice as stiff than CFD [10, 60, 77]. The neonatal porcine LVFW (140 kPa) has the approximately one-third stiffness of equivalent adult porcine (400 kPa) in the MFD [78]. Biaxial extension tends to demonstrate greater stiffness than the uniaxial extension in MFD, with the RVFW exhibiting peak Engineering stress almost double the uniaxial data (Tables 4 and 6). Similarly, biaxial tests show greater anisotropy between MFD and CFD than equivalent uniaxial tests (Figs. 4 & 5), as a consequence of the collagen/muscle fibre crosslinking mechanism.

The RVFW is the stiffest tissue in simple shear, with the MFD stiffer than the CFD. Strain softening was briefly observed, perhaps caused by a disruption of perimysial collagen during cyclic shearing, as a consequence of excessive shearing between adjacent myocardial muscle layers [79-81]. The anterior walls were stiffest with greater energy dissipation, which is again consistent with the relative microstructures (Fig. 3 and Table 2). The greater magnitude of energy dissipation achieved versus biaxial tests (Tables 5 & 7) would appear indicative of the importance of shearing within the heart wall. This attribute is believed to be as a consequence of the relatively high water content of myocardium (~ 80% wet weight) and affected by the muscle presence [64]. The anterior and posterior LVFWs demonstrate similar mechanical trends in the positive and negative directions. The anterior RVFW exhibits a stiffer response in the positive direction, whilst the posterior RVFW has greater stiffness in the negative direction (Fig. 6). Fibre orientation analysis revealed orthogonal alignment of the LVFW muscle fibres, with fibres from the anterior region aligned horizontally and posterior fibres vertically (Figs. 3 (a) & (b), and Table 1). Conversely, the fibres in the anterior and posterior RVFW were aligned nearer diagonally, with the former possessing greater concentration with less intercellular space, which may in part contribute to the RVFWs asymmetric shear behaviour (Table 2 & Fig. 3). The principal or preferred fibre angles were calculated using Fourier component image analysis (Table 1). The stiffness of LVFW adult porcine data has previously been reported at 50% strain as ~ 28 kPa (MFD) and ~ 5 kPa (CFD) [9]. Compared to the equivalent data reported here for neonatal

porcine tissue (i.e. ~ 7.2 kPa (MFD) and ~ 4.2 kPa (CFD) at 50% strain), indicates that the neonatal tissue is approximately one-fourth the stiffness of mature tissue in the MFD. Comparing the stress-strain plots of this shear data, to the above uniaxial data, highlights a similar stress after which the MFD tissue from both ventricles stiffens dramatically (Figs. 4 (a) and 7 (c), (d), (e), (f)). This is consistent with the trend previously reported in adult porcine cardiac tissue [9].

4.1. Limitations

Whilst the above results provide a valuable insight into neonatal cardiac tissue behaviour, it is acknowledged that an animal-based laboratory study differs from human, physiological reality. The porcine model was adopted as the adult organ is commonly used to simulate human performance, given their relatively similar structure and dimensions; however, there are still differences that will limit the applicability of these data. Whilst the controlled environment of a laboratory has significant advantages when investigating tissue characteristics, the need to dissect samples does create artificial boundary conditions and release residual stresses, which may alter performance. Common protocols were followed to ensure the tissues remained hydrated and in a condition similar to their in vivo physiology.

5. Conclusion

A series of mechanical tests have been performed to characterise the behaviour of LVFW and RVFW from the neonatal porcine tissue. A strong correlation is reported between microstructure and mechanical function, whilst the tissue was found to exhibit non–linear, anisotropic, viscoelastic (hysteresis formation) and heterogeneous behaviour. The neonatal tissue is also identified as exhibiting one-half the stiffness of mature porcine tissue in uniaxial testing, one-third in biaxial testing, and one-fourth stiffness in simple shear testing. Hence, these data provide both a baseline describing the biomechanical behaviour of immature porcine cardiac tissue and an indication as to the relative change in characteristics associated with tissue maturation. This may prove valuable to researchers investigating cardiac mechanics.

6. Acknowledgements

FA is grateful to the Ser Cymru NRN in Advanced Engineering & Materials for funding his PhD scholarship. JL is supported in part by NIH 1R01EB022018-01.

References

[1] H. Dolk, M. Loane, E. Garne, The prevalence of congenital anomalies in Europe, Advances in experimental medicine and biology 686 (2010) 349-64.
[2] H. Dolk, M. Loane, E. Garne, G. European Surveillance of Congenital Anomalies Working, Congenital heart defects in Europe: prevalence and perinatal mortality, 2000 to 2005, Circulation 123(8) (2011) 841-9.
[3] L.L. Demer, F.C. Yin, Passive biaxial mechanical properties of isolated canine myocardium, The Journal of physiology 339 (1983) 615-30.
[4] J.D. Humphrey, R.K. Strumpf, F.C.P. Yin, Determination of a Constitutive Relation for Passive Myocardium: II.—Parameter Estimation, Journal of biomechanical engineering 112(3) (1990) 340-346.
[5] V.P. Novak, F.C. Yin, J.D. Humphrey, Regional mechanical properties of passive myocardium, Journal of biomechanics 27(4) (1994) 403-12.
[6] M.S. Sacks, C.J. Chuong, Biaxial Mechanical Properties of Passive Right Ventricular Free Wall Myocardium, Journal of biomechanical engineering 115(2) (1993) 202-205.
[7] F.C. Yin, R.K. Strumpf, P.H. Chew, S.L. Zeger, Quantification of the mechanical properties of noncontracting canine myocardium under simultaneous biaxial loading, Journal of biomechanics 20(6) (1987) 577-89.
[8] M.R. Hill, M.A. Simon, D. Valdez-Jasso, W. Zhang, H.C. Champion, M.S. Sacks, Structural and mechanical adaptations of right ventricle free wall myocardium to pressure overload, Ann Biomed Eng 42(12) (2014) 2451-65.
[9] S. Dokos, B.H. Smaill, A.A. Young, I.J. LeGrice, Shear properties of passive ventricular myocardium, American journal of physiology. Heart and circulatory physiology 283(6) (2002) H2650-9.
[10] G. Sommer, A.J. Schriefl, M. Andrä, M. Sacherer, C. Viertler, H. Wolinski, G.A. Holzapfel, Biomechanical properties and microstructure of human ventricular myocardium, Acta biomaterialia 24 (2015) 172-192.
[11] V. Carapella, R. Bordas, P. Pathmanathan, M. Lohezic, J.E. Schneider, P. Kohl, K. Burrage, V. Grau, Quantitative study of the effect of tissue microstructure on contraction in a computational model of rat left ventricle, PloS one 9(4) (2014) e92792.

[12] P. Helm, M.F. Beg, M.I. Miller, R.L. Winslow, Measuring and mapping cardiac fiber and laminar architecture using diffusion tensor MR imaging, Annals of the New York Academy of Sciences 1047 (2005) 296-307.
[13] W.J. Karlon, A.D. McCulloch, J.W. Covell, J.J. Hunter, J.H. Omens, Regional dysfunction correlates with myofiber disarray in transgenic mice with ventricular expression of ras, American journal of physiology. Heart and circulatory physiology 278(3) (2000) H898-906.
[14] A. Palit, S.K. Bhudia, T.N. Arvanitis, G.A. Turley, M.A. Williams, Computational modelling of left-ventricular diastolic mechanics: effect of fibre orientation and right-ventricle topology, Journal of biomechanics 48(4) (2015) 604-12.
[15] D.D. Streeter, Jr., H.M. Spotnitz, D.P. Patel, J. Ross, Jr., E.H. Sonnenblick, Fiber orientation in the canine left ventricle during diastole and systole, Circulation research 24(3) (1969) 339-47.
[16] C.J. Cote, A practice of anesthesia for infants and children, WB Saunders Company1993.
[17] R.G. Cox, Smith's Anesthesia for Infants and Children - Eighth Edition, Canadian Journal of Anesthesia/Journal canadien d'anesthésie 58(10) (2011) 973.
[18] P. Anversa, J.M. Capasso, Cellular basis of aging in the mammalian heart, Scanning microscopy 5(4) (1991) 1065-73; discussion 1073-4.
[19] C.R. Gazoti Debessa, L.B. Mesiano Maifrino, R. Rodrigues de Souza, Age related changes of the collagen network of the human heart, Mechanisms of Ageing and Development 122(10) (2001) 1049-1058.
[20] C.T. Nguyen, C.S. Hall, M.J. Scott, Q. Zhu, J. Marsh, S.A. Wickline, Age-related alterations of cardiac tissue microstructure and material properties in Fischer 344 rats, Ultrasound in Medicine & Biology 27(5) (2001) 611-619.
[21] M.L. Lindsey, D.K. Goshorn, C.E. Squires, G.P. Escobar, J.W. Hendrick, J.T. Mingoia, S.E. Sweterlitsch, F.G. Spinale, Age-dependent changes in myocardial matrix metalloproteinase/tissue inhibitor of metalloproteinase profiles and fibroblast function, Cardiovascular research 66(2) (2005) 410-419.
[22] S. Giannico, F. Hammad, A. Amodeo, G. Michielon, F. Drago, A. Turchetta, R. Di Donato, S.P. Sanders, Clinical outcome of 193 extracardiac Fontan patients: the first 15 years, Journal of the American College of Cardiology 47(10) (2006) 2065-73.
[23] E. Petrossian, V.M. Reddy, D.B. McElhinney, G.P. Akkersdijk, P. Moore, A.J. Parry, L.D. Thompson, F.L. Hanley, Early results of the extracardiac conduit Fontan operation, The Journal of thoracic and cardiovascular surgery 117(4) (1999) 688-96.
[24] T. Shinoka, C. Breuer, Tissue-engineered blood vessels in pediatric cardiac surgery, The Yale journal of biology and medicine 81(4) (2008) 161-6.
[25] S. Dokos, I.J. LeGrice, B.H. Smaill, J. Kar, A.A. Young, A Triaxial-Measurement Shear-Test Device for Soft Biological Tissues, Journal of biomechanical engineering 122(5) (2000) 471-478.
[26] T.S. Eriksson, A. Prassl, G. Plank, G.A. Holzapfel, Influence of myocardial fiber/sheet orientations on left ventricular mechanical contraction, Mathematics and Mechanics of Solids (2013) 1081286513485779.
[27] T.S. Eriksson, A.J. Prassl, G. Plank, G.A. Holzapfel, Modeling the dispersion in electromechanically coupled myocardium, International journal for numerical methods in biomedical engineering 29(11) (2013) 1267-84.
[28] M.P. Nash, A.V. Panfilov, Electromechanical model of excitable tissue to study reentrant cardiac arrhythmias, Progress in biophysics and molecular biology 85(2-3) (2004) 501-22.
[29] S. Niederer, L. Mitchell, N. Smith, G. Plank, Simulating a human heart beat with near-real time performance, Frontiers in Physiology 2 (2011) 14.
[30] T.P. Usyk, J.H. Omens, A.D. McCulloch, Regional septal dysfunction in a three-dimensional computational model of focal myofiber disarray, American journal of physiology. Heart and circulatory physiology 281(2) (2001) H506-14.

[31] S.T. Wall, J.C. Walker, K.E. Healy, M.B. Ratcliffe, J.M. Guccione, Theoretical impact of the injection of material into the myocardium: a finite element model simulation, Circulation 114(24) (2006) 2627-35.
[32] E. Petrossian, V.M. Reddy, K.K. Collins, C.B. Culbertson, M.J. MacDonald, J.J. Lamberti, O. Reinhartz, R.D. Mainwaring, P.D. Francis, S.P. Malhotra, D.B. Gremmels, S. Suleman, F.L. Hanley, The extracardiac conduit Fontan operation using minimal approach extracorporeal circulation: early and midterm outcomes, The Journal of thoracic and cardiovascular surgery 132(5) (2006) 1054-63.
[33] C.P. Twine, A.D. McLain, Graft type for femoro-popliteal bypass surgery, The Cochrane database of systematic reviews (5) (2010) CD001487.
[34] X. Wang, P. Lin, Q. Yao, C. Chen, Development of small-diameter vascular grafts, World journal of surgery 31(4) (2007) 682-9.
[35] B. Wang, A. Borazjani, M. Tahai, A.L. Curry, D.T. Simionescu, J. Guan, F. To, S.H. Elder, J. Liao, Fabrication of cardiac patch with decellularized porcine myocardial scaffold and bone marrow mononuclear cells, Journal of biomedical materials research. Part A 94(4) (2010) 1100-10.
[36] H. Kurobe, M.W. Maxfield, C.K. Breuer, T. Shinoka, Concise review: tissue-engineered vascular grafts for cardiac surgery: past, present, and future, Stem cells translational medicine 1(7) (2012) 566-71.
[37] A. Bassols, C. Costa, P.D. Eckersall, J. Osada, J. Sabria, J. Tibau, The pig as an animal model for human pathologies: A proteomics perspective, Proteomics. Clinical applications 8(9-10) (2014) 715-31.
[38] P. Vodicka, K. Smetana, Jr., B. Dvorankova, T. Emerick, Y.Z. Xu, J. Ourednik, V. Ourednik, J. Motlik, The miniature pig as an animal model in biomedical research, Annals of the New York Academy of Sciences 1049 (2005) 161-71.
[39] B. Aigner, S. Renner, B. Kessler, N. Klymiuk, M. Kurome, A. Wünsch, E. Wolf, Transgenic pigs as models for translational biomedical research, Journal of molecular medicine 88(7) (2010) 653-664.
[40] G.W. Almond, Research applications using pigs, Veterinary Clinics of North America: food animal practice 12(3) (1996) 707-716.
[41] S.A. Book, L.K. Bustad, The fetal and neonatal pig in biomedical research, Journal of animal science 38(5) (1974) 997-1002.
[42] D. Cooper, Y. Ye, L. Rolf Jr, N. Zuhdi, The pig as potential organ donor for man, Xenotransplantation, Springer1991, pp. 481-500.
[43] W.R. Douglas, Of pigs and men and research, Origins of life and evolution of biospheres 3(3) (1972) 226-234.
[44] Y. Luo, L. Lin, L. Bolund, T.G. Jensen, C.B. Sørensen, Genetically modified pigs for biomedical research, Journal of inherited metabolic disease 35(4) (2012) 695-713.
[45] G.A. Holzapfel, R.W. Ogden, Constitutive modelling of passive myocardium: a structurally based framework for material characterization, Philosophical transactions. Series A, Mathematical, physical, and engineering sciences 367(1902) (2009) 3445-75.
[46] J.S. Grashow, M.S. Sacks, J. Liao, A.P. Yoganathan, Planar biaxial creep and stress relaxation of the mitral valve anterior leaflet, Ann Biomed Eng 34(10) (2006) 1509-18.
[47] J.S. Grashow, A.P. Yoganathan, M.S. Sacks, Biaixal stress-stretch behavior of the mitral valve anterior leaflet at physiologic strain rates, Ann Biomed Eng 34(2) (2006) 315-25.
[48] Z.Q. Liu, Scale space approach to directional analysis of images, Applied optics 30(11) (1991) 1369-73.
[49] N. Reznikov, R. Almany-Magal, R. Shahar, S. Weiner, Three-dimensional imaging of collagen fibril organization in rat circumferential lamellar bone using a dual beam electron microscope reveals ordered and disordered sub-lamellar structures, Bone 52(2) (2013) 676-683.
[50] N. Reznikov, R. Shahar, S. Weiner, Three-dimensional structure of human lamellar bone: the presence of two different materials and new insights into the hierarchical organization, Bone 59 (2014) 93-104.

[51] S. Javani, M. Gordon, A.N. Azadani, Biomechanical Properties and Microstructure of Heart Chambers: A Paired Comparison Study in an Ovine Model, Annals of biomedical engineering 44(11) (2016) 3266-3283.
[52] G.A. Holzapfel, G. Sommer, P. Regitnig, Anisotropic mechanical properties of tissue components in human atherosclerotic plaques, Journal of biomechanical engineering 126(5) (2004) 657-65.
[53] G. Sommer, P. Regitnig, L. Koltringer, G.A. Holzapfel, Biaxial mechanical properties of intact and layer-dissected human carotid arteries at physiological and supraphysiological loadings, American journal of physiology. Heart and circulatory physiology 298(3) (2010) H898-912.
[54] G.A. Holzapfel, G. Sommer, C.T. Gasser, P. Regitnig, Determination of layer-specific mechanical properties of human coronary arteries with nonatherosclerotic intimal thickening and related constitutive modeling, American journal of physiology. Heart and circulatory physiology 289(5) (2005) H2048-58.
[55] G. Sommer, M. Eder, L. Kovacs, H. Pathak, L. Bonitz, C. Mueller, P. Regitnig, G.A. Holzapfel, Multiaxial mechanical properties and constitutive modeling of human adipose tissue: a basis for preoperative simulations in plastic and reconstructive surgery, Acta biomaterialia 9(11) (2013) 9036-48.
[56] G. Sommer, A. Schriefl, G. Zeindlinger, A. Katzensteiner, H. Ainodhofer, A. Saxena, G.A. Holzapfel, Multiaxial mechanical response and constitutive modeling of esophageal tissues: Impact on esophageal tissue engineering, Acta biomaterialia 9(12) (2013) 9379-91.
[57] D.H. Lin, F.C. Yin, A multiaxial constitutive law for mammalian left ventricular myocardium in steady-state barium contracture or tetanus, Journal of biomechanical engineering 120(4) (1998) 504-17.
[58] H. Ghaemi, K. Behdinan, A.D. Spence, In vitro technique in estimation of passive mechanical properties of bovine heart: Part I. Experimental techniques and data, Medical Engineering & Physics 31(1) (2009) 76-82.
[59] K.B. Gupta, M.B. Ratcliffe, M.A. Fallert, L.H. Edmunds, Jr., D.K. Bogen, Changes in passive mechanical stiffness of myocardial tissue with aneurysm formation, Circulation 89(5) (1994) 2315-26.
[60] M.S. Sacks, C.J. Chuong, Biaxial mechanical properties of passive right ventricular free wall myocardium, J Biomech Eng 115(2) (1993) 202-5.
[61] P. Wang, F. Zhu, N.H. Lee, K. Konstantopoulos, Shear-induced interleukin-6 synthesis in chondrocytes: roles of E prostanoid (EP) 2 and EP3 in cAMP/protein kinase A- and PI3-K/Akt-dependent NF-kappaB activation, The Journal of biological chemistry 285(32) (2010) 24793-804.
[62] D. Valdez-Jasso, M.A. Simon, H.C. Champion, M.S. Sacks, A murine experimental model for the mechanical behaviour of viable right-ventricular myocardium, The Journal of physiology 590(18) (2012) 4571-84.
[63] Y.-C. Fung, Bioviscoelastic solids, Biomechanics, Springer1993, pp. 242-320.
[64] J.D. Humphrey, Cardiovascular Solid Mechanics: Cells, Tissues, and Organs, Springer New York2013.
[65] Y.-C. Fung, Mechanical properties and active remodeling of blood vessels, Biomechanics, Springer1993, pp. 321-391.
[66] R. Avazmohammadi, M.R. Hill, M.A. Simon, W. Zhang, M.S. Sacks, A novel constitutive model for passive right ventricular myocardium: evidence for myofiber-collagen fiber mechanical coupling, Biomech Model Mechanobiol 16(2) (2017) 561-581.
[67] J.E. Bishop, G. Lindahl, Regulation of cardiovascular collagen synthesis by mechanical load, Cardiovascular Research 42(1) (1999) 27-44.
[68] D.D. STREETER, H.M. SPOTNITZ, D.P. PATEL, J. ROSS, E.H. SONNENBLICK, Fiber Orientation in the Canine Left Ventricle during Diastole and Systole, Circulation research 24(3) (1969) 339-347.
[69] G.A. Holzapfel, G. Sommer, C.T. Gasser, P. Regitnig, Determination of layer-specific mechanical properties of human coronary arteries with nonatherosclerotic intimal thickening and related

constitutive modeling, American Journal of Physiology - Heart and Circulatory Physiology 289(5) (2005) H2048-H2058.
[70] G. Sommer, P. Regitnig, L. Költringer, G.A. Holzapfel, Biaxial mechanical properties of intact and layer-dissected human carotid arteries at physiological and supraphysiological loadings, American Journal of Physiology - Heart and Circulatory Physiology 298(3) (2010) H898-H912.
[71] C.A.J. Schulze-Bauer, P. Regitnig, G.A. Holzapfel, Mechanics of the human femoral adventitia including the high-pressure response, American Journal of Physiology - Heart and Circulatory Physiology 282(6) (2002) H2427-H2440.
[72] T.K. Borg, J.B. Caulfield, The collagen matrix of the heart, Fed Proc 40(7) (1981) 2037-2041.
[73] K.T. Weber, W.A. Clark, J.S. Janicki, S.G. Shroff, Physiologic versus pathologic hypertrophy and the pressure-overloaded myocardium, Journal of cardiovascular pharmacology 10 Suppl 6 (1987) S37-50.
[74] K.T. Weber, J.S. Janicki, S.G. Shroff, R. Pick, C. Abrahams, R.M. Chen, R.I. Bashey, Collagen compartment remodeling in the pressure overloaded left ventricle, Journal of Applied Cardiology 3(1) (1988) 37-46.
[75] D. Perie, N. Dahdah, A. Foudis, D. Curnier, Multi-parametric MRI as an indirect evaluation tool of the mechanical properties of in-vitro cardiac tissues, BMC cardiovascular disorders 13 (2013) 24.
[76] M.S. Sirry, J.R. Butler, S.S. Patnaik, B. Brazile, R. Bertucci, A. Claude, R. McLaughlin, N.H. Davies, J. Liao, T. Franz, Characterisation of the mechanical properties of infarcted myocardium in the rat under biaxial tension and uniaxial compression, Journal of the Mechanical Behavior of Biomedical Materials 63 (2016) 252-264.
[77] H. Ghaemi, K. Behdinan, A.D. Spence, In vitro technique in estimation of passive mechanical properties of bovine heart part I. Experimental techniques and data, Med Eng Phys 31(1) (2009) 76-82.
[78] B. Wang, G. Wang, F. To, J.R. Butler, A. Claude, R.M. McLaughlin, L.N. Williams, A.L. de Jongh Curry, J. Liao, Myocardial scaffold-based cardiac tissue engineering: application of coordinated mechanical and electrical stimulations, Langmuir : the ACS journal of surfaces and colloids 29(35) (2013) 11109-17.
[79] J. Emery, J. Omens, O. Mathieu-Costello, A. McCulloch, Structural mechanisms of acute ventricular strain softening, Int J Cardiovasc Med Sci 1 (1998) 241-250.
[80] J.L. Emery, J.H. Omens, A.D. McCulloch, Biaxial mechanics of the passively overstretched left ventricle, The American journal of physiology 272(5 Pt 2) (1997) H2299-305.
[81] J.L. Emery, J.H. Omens, A.D. McCulloch, Strain softening in rat left ventricular myocardium, Journal of biomechanical engineering 119(1) (1997) 6-12.

Graphical abstract